Large linear and nonlinear electro-optic coefficients in two-dimensional ferroelectrics

Zhijun Jiang, Charles Paillard, Hugh O H Churchill, Minggang Xia, Shengli Zhang, Hongjun Xiang, L. Bellaiche

▶ **To cite this version:**

Zhijun Jiang, Charles Paillard, Hugh O H Churchill, Minggang Xia, Shengli Zhang, et al.. Large linear and nonlinear electro-optic coefficients in two-dimensional ferroelectrics. Physical Review B, 2022, 106 (8), pp.L081404. 10.1103/PhysRevB.106.L081404 . hal-03767985

HAL Id: hal-03767985

https://centralesupelec.hal.science/hal-03767985

Submitted on 2 Sep 2022

HAL is a multi-disciplinary open access archive for the deposit and dissemination of scientific research documents, whether they are published or not. The documents may come from teaching and research institutions in France or abroad, or from public or private research centers.

L'archive ouverte pluridisciplinaire **HAL**, est destinée au dépôt et à la diffusion de documents scientifiques de niveau recherche, publiés ou non, émanant des établissements d'enseignement et de recherche français ou étrangers, des laboratoires publics ou privés.

Large linear and nonlinear electro-optic coefficients in two-dimensional ferroelectrics

Zhijun Jiang,[1,2,3,*] Charles Paillard,[3,4,*] Hugh O. H. Churchill,[3]
Minggang Xia,[1] Shengli Zhang,[1] Hongjun Xiang,[2,5,6,†] and L. Bellaiche[3,‡]

[1]*MOE Key Laboratory for Nonequilibrium Synthesis and Modulation of Condensed Matter, Shaanxi Province Key Laboratory of Advanced Functional Materials and Mesoscopic Physics, School of Physics, Xi'an Jiaotong University, Xi'an 710049, China*
[2]*Key Laboratory of Computational Physical Sciences (Ministry of Education), State Key Laboratory of Surface Physics, and Department of Physics, Fudan University, Shanghai 200433, China*
[3]*Physics Department and Institute for Nanoscience and Engineering, University of Arkansas, Fayetteville, Arkansas 72701, USA*
[4]*Laboratoire SPMS, CentraleSupélec/CNRS UMR 8580, Université Paris-Saclay, 8-10 rue Joliot Curie, 91190 Gif-sur-Yvette, France*
[5]*Collaborative Innovation Center of Advanced Microstructures, Nanjing 210093, China*
[6]*Shanghai Qi Zhi Institute, Shanghai 200030, China*

Analytical derivations and first-principles calculations are performed to investigate the electro-optic (EO) response of the two-dimensional ferroelectric SnS in its monolayer form. In addition to derive the formula for EO coefficients for two-dimensional systems, large linear and nonlinear electro-optic coefficients are discovered, along with a strongly nonlinear electro-optic response as a function of electric field. The origin of these electro-optic responses is further found and involves a few specific phonon modes, in general, and the evolution of their frequencies and atomic characteristics under electric fields, in particular. Large linear and nonlinear electro-optic coefficients can be found in other two-dimensional ferroelectrics, paving the way for potential optical device applications.

The electro-optic (EO) effect characterizes the change in refractive index of a material induced by an applied static (or low-frequency) electric field [1], which can be used for some technological applications [2–7]. As such, EO effects have been intensively studied in recent years (see, e.g., Refs. [8–22] and references therein). In particular, obtaining large *linear* but also *nonlinear* electro-optic coefficients are required for designing efficient and/or novel optical devices, including EO modulation [10], optical shutters [15], EO detection [17], and EO switching [19]. Interestingly, EO effects have been exploited in graphene for EO modulators [23], indicating the possibility of using two-dimensional (2D) materials for the design of such novel devices. Similarly, a few recent experiments have been conducted on EO effects in molecular ferroelectrics [24] and ferroelectric HfO_2-based epitaxial thin films [25]. On the other hand, we are not aware of any study devoted to EO effects in many other 2D ferroelectric materials, despite a current intensive research conducted in such promising nanostructures. Examples of such systems are, e.g., 1T′-WTe_2 [26], *d*1T-$MoTe_2$ [27], $CuInP_2S_6$ [28], bilayer *h*-BN [29, 30] and transition metal dichalcogenides [31] for which the direction of the spontaneous polarization can be out-of plane, or SnTe [32], β'-In_2Se_3 [33], SnSe [34] and SnS [35] that exhibit an in-plane polarization. In particular, SnS is attracting much attention [35–45], because it is chemically stable and exhibits a robust room-temperature ferroelectricity even in its monolayer form—which is highly promising for nanoscale ferroelectric applications [35]. It is thus timely and important to know if SnS monolayer possesses large linear and nonlinear electro-optic coefficients, and, if yes, what are the microscopic reasons behind them. One may also wonder how to practically compute EO coefficients in 2D materials since the only available *ab-initio* method allowing the determination of such coefficients pertains to the simulations of *supercells* [12].

The aim of this Letter is to report derivations and first-principles calculations that positively answer such questions and provide a deep insight into these EO responses.

Here, we choose the ground state structure of SnS monolayer, which has a $Pmn2_1$ symmetry. The spontaneous polarization in this structure is along the armchair direction, as theoretically and experimentally demonstrated [35, 43]. We perform density functional theory (DFT) calculations within the generalized gradient approximation in the form of Perdew-Burke-Ernzerhof (PBE) exchange-correlation functional [46], using the ABINIT package [47] with norm-conserving pseudopotentials [48, 49]. We used a Γ-centered $10 \times 10 \times 1$ grid of k-point mesh and a plane-wave cutoff of 50 hartrees. A vacuum space of more than 65 Å is employed to avoid the periodic image interactions and to get converged EO coefficients. In addition, the Coulomb interaction in 2D system is naturally included in our DFT calculations. The effects of dc electric fields applied along the [100] armchair polar direction on structural properties of the $Pmn2_1$ phase of monolayer SnS are calculated by making full use of the method developed in Refs. [50–52]. Note that, for each considered magnitude of the dc electric field, the in-plane lattice vectors were allowed to relax while the out-of-plane lattice vector was kept fixed (in order to have a constant width of the vacuum layer), and the atomic positions were fully relaxed until all the forces acting on the atoms have a value smaller than 1×10^{-6} hartrees/bohr. The resulting field-induced structures are then used to obtain the EO coefficients, which is based on the variations of the refractive index (related to the first-order change of the optical dielectric tensor) induced by a static (or low frequency) electric field $\mathcal{E}_k$ [53]. More precisely, the EO coefficients are computed within the density functional pertur-

bation theory (DFPT) on those field-induced structures, which has been previously demonstrated to give rise to correct nonlinear electro-optic coefficients [22]. Technically, the EO coefficients can be obtained from the following expression:

$$\Delta(\varepsilon^{-1})_{ij} = \sum_{k=1}^{3} \mathcal{R}_{ijk}\mathcal{E}_k, \tag{1}$$

where $(\varepsilon^{-1})_{ij}$ is the inverse of the electronic dielectric tensor and $\mathcal{R}_{ijk}$ is the EO tensor, with both of these quantities implicitly depending on the applied field, $\mathcal{E}_k$. The relationship between $\mathcal{R}_{ijk}$ and $\mathcal{E}_k$ will determine if the considered materials adopt a linear or nonlinear EO effects.

Let us consider the clamped (strain-free) EO tensor *for the supercell* (that contains both the monolayer and the vacuum layers), $\mathcal{R}^{\eta,\mathrm{SC}}_{ijk}$ (note the superscript "SC" that refers to the supercell). It can be expressed as the sum of two contributions: a bare part $\mathcal{R}^{\mathrm{el,SC}}_{ijk}$, and an ionic contribution $\mathcal{R}^{\mathrm{ion,SC}}_{ijk}$ [12, 13]. The electronic part can be computed from the nonlinear optical coefficients while the ionic contribution is related to the Raman susceptibility α^m_{ij} of mode m, the transverse optic (TO) mode polarity p^m_k and the TO phonon mode frequencies ω_m. More precisely, the clamped EO tensor for the supercell is written as [12, 13, 22]:

$$\mathcal{R}^{\eta,\mathrm{SC}}_{ijk} = \mathcal{R}^{\mathrm{el,SC}}_{ijk} + \mathcal{R}^{\mathrm{ion,SC}}_{ijk} = \frac{-8\pi}{n_i^2 n_j^2}\chi^{(2)}_{ijk} - \frac{4\pi}{n_i^2 n_j^2\sqrt{\Omega_0}}\sum_m \frac{\alpha^m_{ij}p^m_k}{\omega^2_m}, \tag{2}$$

where the n_i and n_j coefficients are the principal refractive indices, and Ω_0 is the unit-cell volume. Note that we decided to focus on clamped EO coefficients here, rather than on the unclamped ones, for three main reasons: (1) as we will see below, Eq. (2) can provide a deep insight into the electro-optic response; (2) measurements, known as the Time Response Method (TRM), can be done to extract such clamped coefficients [54, 55]; and (3) clamped and unclamped coefficients can be mixed in the electro-optic response of some devices [56, 57]. Note also that one "just" has to add contributions associated with elasto-optic and piezoelectric coefficients to obtain the unclamped EO responses from the clamped ones [11–13].

We first check the structural parameters of *bulk* SnS (that has a $Pnma$ space group). The presently used PBE exchange-correlation energy functional [48, 49] provides a, b and c lattice constants equal to 4.45, 4.03 and 11.43 Å, respectively, which typically slightly overestimates (between 1.0 and 2.8%) the corresponding experimental values of 4.33, 3.99 and 11.20 Å [58].

Figure 1(a) depicts the crystal structure of SnS *monolayer* in its $Pmn2_1$ ground state under zero field. A spontaneous polarization exists along the armchair direction (note that the polarization P is computed from the Berry phase method [59, 60]), with a value of 268 pC/m, which is in good agreement with the previous theoretical values of 265 pC/m [45], 262 pC/m [38], and 260 pC/m [40]. Note that a measurement provides a magnitude higher by four orders of magnitude, i.e., ∼3 μC/m, but noted that the discrepancy between

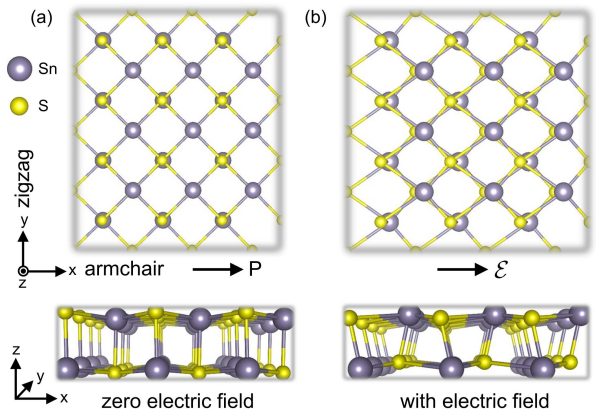

FIG. 1. Crystal structures of the monolayer SnS. Panel (a) depicts the top and side views of monolayer SnS with zero electric field. Panel (b) displays the top and side views of monolayer SnS with the largest applied electric field ≃4.6 × 10^8 V/m.

the predicted and experimental values may arise from an observed hysteresis loop that is dominantly caused by extrinsic effects [35]. Figure 1(b) shows a similar $Pmn2_1$ structure but under our largest applied electric field. We choose here the Cartesian axes such as the x-axis is along the [100] polar pseudo-cubic direction (armchair direction in Fig. 1), the y-axis is along the [010] of the pseudo-cubic direction (zigzag direction in Fig. 1), and the z-axis is perpendicular to the spanned (x, y) plane. With this choice of axes and within the $Pmn2_1$ (C_{2v}) symmetry, the EO tensor has five independent elements in Voigt notation [61]: $\mathcal{R}_{11}$, $\mathcal{R}_{21}$, $\mathcal{R}_{31}$, $\mathcal{R}_{53}$ and $\mathcal{R}_{62}$. It is now important to realize that we want to compute the EO coefficients of the monolayer (to be later referred by using the "2D" superscript), while the *ab-initio* code provides the EO coefficients and the dielectric tensor of the whole supercell (that also contains vacuum layers). The Supplemental Material (SM) [62] provides the necessary derivations and gives

$$\mathcal{R}^{\eta,\mathrm{2D}}_{11}(\mathcal{E}) = \frac{c}{t}\frac{\left(\varepsilon^{\mathrm{SC}}_{11}\right)^2}{\left(\varepsilon^{\mathrm{2D}}_{11}\right)^2}\mathcal{R}^{\eta,\mathrm{SC}}_{11}(\mathcal{E}), \tag{3}$$

$$\mathcal{R}^{\eta,\mathrm{2D}}_{21}(\mathcal{E}) = \frac{c}{t}\frac{\left(\varepsilon^{\mathrm{SC}}_{22}\right)^2}{\left(\varepsilon^{\mathrm{2D}}_{22}\right)^2}\mathcal{R}^{\eta,\mathrm{SC}}_{21}(\mathcal{E}), \tag{4}$$

$$\mathcal{R}^{\eta,\mathrm{2D}}_{31}(\mathcal{E}) = \frac{c}{t}\mathcal{R}^{\eta,\mathrm{SC}}_{31}(\mathcal{E}), \tag{5}$$

$$\mathcal{R}^{\eta,\mathrm{2D}}_{53}(\mathcal{E}) = \frac{\varepsilon^{\mathrm{SC}}_{33}\varepsilon^{\mathrm{SC}}_{11}}{\varepsilon^{\mathrm{2D}}_{33}\varepsilon^{\mathrm{2D}}_{11}}\mathcal{R}^{\eta,\mathrm{SC}}_{53}(\mathcal{E}), \tag{6}$$

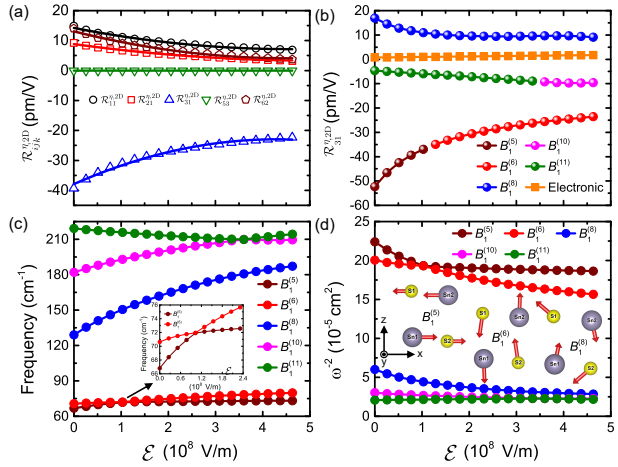

FIG. 2. (a) The clamped 2D EO coefficients as a function of electric field applied along the [100] direction in monolayer SnS. The solid lines represent fits by a second-order polynomial except for $\mathcal{R}^{\eta,\mathrm{2D}}_{53}$ (green line) for which a first-order polynomial was fit to. (b) Mode decomposition of the clamped EO coefficient $\mathcal{R}^{\eta,\mathrm{2D}}_{31}$. (c) Phonon frequency for $B_1^{(5)}$, $B_1^{(6)}$, $B_1^{(8)}$, $B_1^{(10)}$ and $B_1^{(11)}$ modes at the Γ point of the first Brillouin zone (the inset zooms in the data of $B_1^{(5)}$ and $B_1^{(6)}$ modes for electric field between 0.0 $\times$ 10^8 V/m and 2.4 $\times$ 10^8 V/m). (d) The inverse of the square of the phonon frequency, ω^{-2}, as a function of electric field. The insets of panel (d) corresponding to the eigenvector of $B_1^{(5)}$, $B_1^{(6)}$ and $B_1^{(8)}$ modes at zero field in monolayer SnS.

$$\mathcal{R}^{\eta,\mathrm{2D}}_{62}(\mathcal{E}) = \frac{c}{t}\frac{\varepsilon^{\mathrm{SC}}_{11}\varepsilon^{\mathrm{SC}}_{22}}{\varepsilon^{\mathrm{2D}}_{11}\varepsilon^{\mathrm{2D}}_{22}}\mathcal{R}^{\eta,\mathrm{SC}}_{62}(\mathcal{E}), \tag{7}$$

where $\mathcal{R}^{\eta,\mathrm{2D}}_{11}$, $\mathcal{R}^{\eta,\mathrm{2D}}_{21}$, $\mathcal{R}^{\eta,\mathrm{2D}}_{31}$, $\mathcal{R}^{\eta,\mathrm{2D}}_{53}$ and $\mathcal{R}^{\eta,\mathrm{2D}}_{62}$ are the clamped 2D EO coefficients; $\mathcal{R}^{\eta,\mathrm{SC}}_{11}$, $\mathcal{R}^{\eta,\mathrm{SC}}_{21}$, $\mathcal{R}^{\eta,\mathrm{SC}}_{31}$, $\mathcal{R}^{\eta,\mathrm{SC}}_{53}$ and $\mathcal{R}^{\eta,\mathrm{SC}}_{62}$ form the clamped EO tensor of the supercell; $\varepsilon^{\mathrm{SC}}_{11}$, $\varepsilon^{\mathrm{SC}}_{22}$ and $\varepsilon^{\mathrm{SC}}_{33}$ are the diagonal elements of the dielectric tensor in the supercell; $\varepsilon^{\mathrm{2D}}_{11}$, $\varepsilon^{\mathrm{2D}}_{22}$ and $\varepsilon^{\mathrm{2D}}_{33}$ are the 2D dielectric constants; c is the thickness of the supercell (out-of-plane lattice constant of the supercell containing both the monolayer SnS and vacuum layer thickness) while t is the effective thickness of the 2D material. Practically, we consider here an out-of-plane lattice constant of the supercell c = 70 Å and a real SnS monolayer thickness of t = 2.6 Å. Note that, as also reported in the Supplemental Material, the relations between the 2D dielectric constants and the dielectric tensor of the supercell are given by [63]: $\varepsilon^{\mathrm{2D}}_{11} = 1 + \frac{c}{t}\left(\varepsilon^{\mathrm{SC}}_{11} - 1\right)$, $\varepsilon^{\mathrm{2D}}_{22} = 1 + \frac{c}{t}\left(\varepsilon^{\mathrm{SC}}_{22} - 1\right)$, and $\varepsilon^{\mathrm{2D}}_{33} = \left[1 + \frac{c}{t}\left(\left(\varepsilon^{\mathrm{SC}}_{33}\right)^{-1} - 1\right)\right]^{-1}$.

Figure 2(a) displays all 2D EO coefficients as a function of the dc electric field applied along the [100] direction in monolayer SnS, as calculated from Eqs. (3)-(7).

One can see a strong field-dependency of $\mathcal{R}^{\eta,\mathrm{2D}}_{31}$, while $\mathcal{R}^{\eta,\mathrm{2D}}_{11}$, $\mathcal{R}^{\eta,\mathrm{2D}}_{21}$, $\mathcal{R}^{\eta,\mathrm{2D}}_{53}$, and $\mathcal{R}^{\eta,\mathrm{2D}}_{62}$ are only weakly (and nearly linearly) dependent on the applied electric field. More precisely, $\mathcal{R}^{\eta,\mathrm{2D}}_{31}$ can be nicely fitted by a second-order polynomial: $r^{\eta,\mathrm{2D}}_{31} + s^{\eta,\mathrm{2D}}_{311}\mathcal{E}_1 + c^{\eta,\mathrm{2D}}_{3111}\mathcal{E}_1^2$, with a linear (Pockels effect) EO coefficient of $r^{\eta,\mathrm{2D}}_{31} = -40.0$ pm/V, a second-order (Kerr effect) EO coefficient of $s^{\eta,\mathrm{2D}}_{311} = 7.0 \times 10^{-20}$ m^2/V^2, and a third-order EO coefficient of $c^{\eta,\mathrm{2D}}_{3111} = -8.1 \times 10^{-29}$ m^3/V^3. Interestingly, $r^{\eta,\mathrm{2D}}_{31}$ is a large linear EO coefficient, since it is very close in magnitude to the one measured in the $P4mm$ phase of $BaTiO_3$ (40.6 pm/V) [11]. Note that, to the best of our knowledge, the largest linear EO coefficient was measured in strontium barium niobate $Sr_{0.6}Ba_{0.4}NbO_6$ single crystal ($4mm$ point group) and is equal to 237 pm/V at room temperature [64], which is about 6 times larger than our predicted value of 40 pm/V at 0 K. This is quite remarkable when realizing that linear EO coefficient should increase when heating the system towards the paraelectric-to-ferroelectric transition [14, 65]. It is thus probable that SnS monolayer can have very large linear EO coefficients at finite temperature. Note also that our estimated $s^{\eta,\mathrm{2D}}_{311}$ quadratic EO parameter is the same order in magnitude than that predicted for the $R3m$ phase of $BaTiO_3$ [22], and about two times stronger than that of potassium dihydrogen phosphate (KDP) [66]. In contrast, $\mathcal{R}^{\eta,\mathrm{2D}}_{53}$ is rather small (approaching a zero value) for all applied fields.

Furthermore, we also numerically found that $\mathcal{R}^{\eta,\mathrm{2D}}_{11}$, $\mathcal{R}^{\eta,\mathrm{2D}}_{21}$ and $\mathcal{R}^{\eta,\mathrm{2D}}_{62}$ can also be very well fitted by second-order polynomials $r^{\eta,\mathrm{2D}}_{11} + s^{\eta,\mathrm{2D}}_{111}\mathcal{E}_1 + c^{\eta,\mathrm{2D}}_{1111}\mathcal{E}_1^2$, $r^{\eta,\mathrm{2D}}_{21} + s^{\eta,\mathrm{2D}}_{211}\mathcal{E}_1 + c^{\eta,\mathrm{2D}}_{2111}\mathcal{E}_1^2$ and $r^{\eta,\mathrm{2D}}_{62} + s^{\eta,\mathrm{2D}}_{621}\mathcal{E}_1 + c^{\eta,\mathrm{2D}}_{6211}\mathcal{E}_1^2$, respectively. The resulting fitting coefficients are: $r^{\eta,\mathrm{2D}}_{11} = 14.2$ pm/V, $s^{\eta,\mathrm{2D}}_{111} = -3.1 \times 10^{-20}$ m^2/V^2, and $c^{\eta,\mathrm{2D}}_{1111} = 3.4 \times 10^{-29}$ m^3/V; $r^{\eta,\mathrm{2D}}_{21} = 8.8$ pm/V, $s^{\eta,\mathrm{2D}}_{211} = -2.2 \times 10^{-20}$ m^2/V^2, and $c^{\eta,\mathrm{2D}}_{2111} = 2.1 \times 10^{-29}$ m^3/V; and $r^{\eta,\mathrm{2D}}_{62} = 13.1$ pm/V, $s^{\eta,\mathrm{2D}}_{621} = -4.0 \times 10^{-20}$ m^2/V^2, and $c^{\eta,\mathrm{2D}}_{6211} = 4.4 \times 10^{-29}$ m^3/V. It is also clear from Fig. 2(a) that one needs to go beyond quadratic EO coefficients to fit well the field-evolution of $\mathcal{R}^{\eta,\mathrm{2D}}_{ijk}$ elements (such evolution will simply be linear if quadratic EO coefficients will suffice), therefore emphasizing the strong nonlinear character of the electro-optic response in SnS monolayer. We are not aware of any previous study reporting significant high-order electro-optic coefficients in any material, beyond quadratic ones. Note that we also checked the spin-orbit coupling (SOC) in 2D ferroelectric SnS monolayer, which has only a small effect on the structural parameters and 2D EO coefficients.

Let us now try to reveal the origin of the large nonlinear EO behaviors in monolayer SnS. For that, we focused on the largest EO coefficient, that is $\mathcal{R}^{\eta,\mathrm{2D}}_{31}$. Since Eq. (5) shows that $\mathcal{R}^{\eta,\mathrm{2D}}_{31}$ is proportional to the clamped EO coefficient of the supercell $\mathcal{R}^{\eta,\mathrm{SC}}_{31}$, one can thus use Eq. (2), and multiply it by c/t to analyze $\mathcal{R}^{\eta,\mathrm{2D}}_{31}$. We thus consider the contribution of each zone-center phonon mode on it (that are the m modes in Eq. (2) and are directly obtained from DFPT calculations [13]). Figure 2(b) shows its decomposition into the $B_1^{(5)}$, $B_1^{(6)}$, $B_1^{(8)}$, $B_1^{(10)}$ and $B_1^{(11)}$ modes, along with its electronic contribution. The electronic contribution is only weakly dependent on the applied electric field, which varies from 0.7

to 1.7 pm/V when the field increases from 0.0 to 4.6 $\times$ 10^8 V/m. Note that the inset of Fig. 2(d) provides insight into the atomic character of some of these modes at zero field. For instance, the Sn1 and S2 ions belonging to the bottom layer move along the in-plane [100] direction while Sn2 and S1 ions in the top layer are displaced along the opposite [$\bar{1}$00] direction in the $B_1^{(5)}$ mode. In contrast, Sn1 and S1 ions mainly have motions along the out-of-plane [00$\bar{1}$] direction, and Sn2 and S2 ions move along the opposite [001] direction in the $B_1^{(6)}$ mode. For the $B_1^{(8)}$ mode, Sn1 and Sn2 ions have both in-plane and out-of-plane displacements (they mainly move along [101] and [10$\bar{1}$] directions) while S1 and S2 ions are displaced along [$\bar{1}$01] and [$\bar{1}$0$\bar{1}$] directions, respectively. Figure 2(b) reveals two important features: (1) $B_1^{(5)}$, $B_1^{(6)}$ and $B_1^{(8)}$ are the dominant modes in the total $\mathcal{R}_{31}^{\eta,2D}$ EO response; and (2) there is an anticrossing between the $B_1^{(5)}$ and $B_1^{(6)}$ modes for a field close to $\simeq$1.0 $\times$ 10^8 V/m (to be discussed in more details later on, and that naturally results in the eigenvectors of $B_1^{(5)}$ and $B_1^{(6)}$ modes inverting their atomic displacement pattern before *versus* after this critical field [21]). In fact, one can gather the combined contributions of $B_1^{(5)}$ and $B_1^{(6)}$ in the entire field range and obtain a second-order polynomial $r_{31}^{\eta,2D} + s_{311}^{\eta,2D}\mathcal{E}_1 + c_{3111}^{\eta,2D}\mathcal{E}_1^2$, with $r_{31}^{\eta,2D} = -50$ pm/V, $s_{311}^{\eta,2D} = 1.2 \times 10^{-19}$ m^2/V^2, and $c_{3111}^{\eta,2D} = -1.5 \times 10^{-28}$ m^3/V^3. Furthermore the separate contribution of the $B_1^{(8)}$ mode provides a similar analytical expression, but with $r_{31}^{\eta,2D} = 15.3$ pm/V, $s_{311}^{\eta,2D} = -4.0\times 10^{-20}$ m^2/V^2, and $c_{3111}^{\eta,2D} = 6.4 \times 10^{-29}$ m^3/V^3. By comparing with the aforementioned second-order polynomial for the *total* $\mathcal{R}_{31}^{\eta,2D}$, one can then deduce that the contribution of the combined $B_1^{(5)}$ and $B_1^{(6)}$ modes (respectively, of the single $B_1^{(8)}$ mode) to the (i) linear EO coefficient $r_{31}^{\eta,2D}$ is 125% (respectively, -38%); (ii) the second-order EO coefficient $s_{311}^{\eta,2D}$ is 171% (respectively, -57%); and (iii) the third-order EO coefficient $c_{3111}^{\eta,2D}$ is 185% (respectively, -79%). Consequently, the whole EO response basically arises from $B_1^{(5)}$, $B_1^{(6)}$ and $B_1^{(8)}$ in the case of $\mathcal{R}_{31}^{\eta,2D}$.

In order to further shed light into these results, Figs. 2(c) and 2(d) show the phonon frequency and inverse of the square of the phonon frequency ω^{-2} as a function of electric field for $B_1^{(5)}$, $B_1^{(6)}$, $B_1^{(8)}$, $B_1^{(10)}$ and $B_1^{(11)}$ modes—because Eq. (2) indicates that the EO coefficient depends on such inverse quantity. Figure 2(d) tells us that the strongly nonlinear $\mathcal{R}_{31}^{\eta,2D}$ EO response of monolayer SnS for fields smaller than $\simeq$1.0 $\times$ 10^8 V/m originates from the inverse of the square of the frequencies of the $B_1^{(5)}$ and $B_1^{(8)}$ modes significantly decreasing with field. However, the anticrossing happening near $\simeq$1.0 $\times$ 10^8 V/m between $B_1^{(5)}$ and $B_1^{(6)}$ makes these modes repelling each other (leading to a gap between their two phonon frequencies and thus the inverse of their square, as clearly seen in Fig. S3 of the SM [62]) and results in $B_1^{(6)}$, rather than $B_1^{(5)}$, having its ω^{-2} being strongly dependent on the electric field above $\simeq$1.0 $\times$ 10^8 V/m. Consequently, for fields larger than 1.0 $\times$ 10^8 V/m, the most important contributions for $\mathcal{R}_{31}^{\eta,2D}$ including its nonlinear EO behavior, now stem from the $B_1^{(6)}$ and $B_1^{(8)}$ modes, via the field-dependency of their resonant frequencies. Note also that, as shown in Figs. 2(c) and 2(d), there is another anticrossing happening under the application of an electric field. It involves the $B_1^{(10)}$ and $B_1^{(11)}$ modes and occurs at a field $\simeq$3.6 $\times$ 10^8 V/m. However, such anticrossing has only small effects on the $\mathcal{R}_{31}^{\eta,2D}$ response because the frequencies of these two modes are much higher than those of $B_1^{(5)}$, $B_1^{(6)}$, $B_1^{(8)}$, as consistent with Eq. (2) indicating that small ω^{-2} leads to weak EO responses.

In summary, based on first-principles calculations, we predict the existence of large linear EO coefficients, accompanied with strong nonlinear electro-optic conversion, in 2D ferroelectric SnS monolayer. Specific phonon modes, having in-plane and/or out-of-plane atomic displacements, have further discovered to be at the origin of these unusually large responses. We also find that other 2D ferroelectrics exhibiting in-plane ferroelectricity, such as SnSe monolayer, can also have large linear and nonlinear EO coefficients, as shown in the SM [62]. Note also that we further computed the EO coefficients of SnS monolayer but under dc electric fields that are opposite to the initial spontaneous polarization's direction. Significant nonlinear and linear EO behaviors are found there too, especially for fields that are close but smaller than the critical field associated with the change of sign of the polarization (see Fig. S4 of the SM [62]). We thus hope that the present study broadens the knowledge of the fascinating and technologically-important research fields devoted to EO effects and 2D materials.

This work is supported by the National Natural Science Foundation of China (Grants No. 11804138, No. 11825403, No. 11774278 and No. 11774280), Shandong Provincial Natural Science Foundation (Grant No. ZR2019QA008), China Postdoctoral Science Foundation (Grants No. 2020T130120 and No. 2018M641905), and "Young Talent Support Plan" of Xi'an Jiaotong University (Grant No. WL6J004). C. P. and L. B. acknowledge ARO Grant No. W911NF-21-1-0113. H. C. and L. B acknowledge the MonArk NSF Quantum Foundry supported by the National Science Foundation Q-AMASE-i program under NSF award No. DMR-1906383. The Arkansas High Performance Computing Center (AHPCC) and the HPC Platform of Xi'an Jiaotong University are also acknowledged.

* These authors contributed equally to this work.
† hxiang@fudan.edu.cn
‡ laurent@uark.edu

[1] M. J. Weber, *Handbook of Optical Materials* (CRC Press, Boca Raton, FL, 2002).
[2] M. E. Lines and A. M. Glass, *Principles and Applications of Ferroelectrics and Related Materials* (Oxford University Press, New York, 1977).
[3] S. H. Wemple and M. DiDomenico, Jr., Electrooptical and Nonlinear Optical Properties of Crystals, Appl. Solid State Sci. **3**, 263 (1972).

[4] B. E. A. Saleh and M. C. Teich, *Fundamentals of Photonics* (Wiley, New York, 1991).

[5] A. Yariv and P. Yeh, *Photonics: Optical Electronics in Modern Communications* (Oxford University Press, New York, 2007).

[6] R. W. Boyd, *Nonlinear Optics*, 3rd ed. (Academic Press, New York, 2008).

[7] M. Bass, *Handbook of Optics: Volume IV-Optical Properties of Materials, Nonlinear Optics, Quantum Optics*, 3rd ed. (McGraw-Hill Education, New York, 2010).

[8] M. DiDomenico, Jr. and S. H. Wemple, Oxygen-octahedra ferroelectrics. I. theory of electro-optical and nonlinear optical effects, J. Appl. Phys. **40**, 720 (1969).

[9] S. H. Wemple and M. DiDomenico, Jr., Oxygen-octahedra ferroelectrics. II. electro-optical and nonlinear-optical device applications, J. Appl. Phys. **40**, 735 (1969).

[10] M. G. Kuzyk, J. E. Sohn, and C. W. Dirk, Mechanisms of quadratic electro-optic modulation of dye-doped polymer systems, J. Opt. Soc. Am. B **7**, 842 (1990).

[11] M. Zgonik, P. Bernasconi, M. Duelli, R. Schlesser, P. Günter, M. H. Garrett, D. Rytz, Y. Zhu, and X. Wu, Dielectric, elastic, piezoelectric, electro-optic, and elasto-optic tensors of $BaTiO_3$ crystals, Phys. Rev. B **50**, 5941 (1994).

[12] M. Veithen, X. Gonze, and Ph. Ghosez, First-Principles Study of the Electro-Optic Effect in Ferroelectric Oxides, Phys. Rev. Lett. **93**, 187401 (2004).

[13] M. Veithen, X. Gonze, and Ph. Ghosez, Nonlinear optical susceptibilities, Raman efficiencies, and electro-optic tensors from first-principles density functional perturbation theory, Phys. Rev. B **71**, 125107 (2005).

[14] M. Veithen and Ph. Ghosez, Temperature dependence of the electro-optic tensor and refractive indices of $BaTiO_3$ from first principles, Phys. Rev. B **71**, 132101 (2005).

[15] Y. Hisakado, H. Kikuchi, T. Nagamura, and T. Kajiyama, Large electro-optic Kerr effect in polymer-stabilized liquid-crystalline blue phases, Adv. Mater. **17**, 96 (2005).

[16] S. Cabuk, The nonlinear optical susceptibility and electro-optic tensor of ferroelectrics: first-principle study, Cent. Eur. J. Phys. **10**, 239 (2012).

[17] R.-L. Jin, Y.-H. Yu, H. Yang, F. Zhu, Q.-D. Chen, M.-B. Yi, and H.-B. Sun, Electro-optical detection based on large Kerr effect in polymer-stabilized liquid crystals, Opt. Lett. **37**, 842 (2012).

[18] L. Chen, Y. Zhang, Q. Guo, D. Zhang, X. Zhong, and J. Yuan, Terahertz electro-optic properties of $PbZr_{0.52}Ti_{0.48}O_3$ and $BaTiO_3$ ferroelectric thin films, Appl. Phys. Lett. **105**, 112903 (2014).

[19] T.-Z. Shen, S.-H. Hong, and J.-K. Song, Electro-optical switching of graphene oxide liquid crystals with an extremely large Kerr coefficient, Nat. Mater. **13**, 394 (2014).

[20] C. Paillard, S. Prokhorenko, and L. Bellaiche, Strain engineering of electro-optic constants in ferroelectric materials, npj Comput. Mater. **5**, 6 (2019).

[21] Z. Jiang, C. Paillard, D. Vanderbilt, H. Xiang, and L. Bellaiche, Designing Multifunctionality via Assembling Dissimilar Materials: Epitaxial AlN/ScN Superlattices, Phys. Rev. Lett. **123**, 096801 (2019).

[22] Z. Jiang, C. Paillard, H. Xiang, and L. Bellaiche, Linear Versus Nonlinear Electro-Optic Effects in Materials, Phys. Rev. Lett. **125**, 017401 (2020).

[23] Z. Sun, A. Martinez, and F. Wang, Optical modulators with 2D layered materials, Nat. Photon. **10**, 227 (2016).

[24] Y. Hu and S. Ren, Electroresistance and electro-optic effects in molecular ferroelectrics, APL Mater. **8**, 080702 (2020).

[25] S. Kondo, R. Shimura, T. Teranishi, A. Kishimoto, T. Nagasaki, H. Funakubo, and T. Yamada, Linear electro-optic effect in ferroelectric HfO_2-based epitaxial thin films, Jpn. J. Appl. Phys. **60**, 070905 (2021).

[26] Z. Fei, W. Zhao, T. A. Palomaki, B. Sun, M. K.Miller, Z. Zhao, J. Yan, X. Xu, and D. H. Cobden, Ferroelectric switching of a two-dimensional metal, Nature (London) **560**, 336 (2018).

[27] S. Yuan, X. Luo, H. L. Chan, C. Xiao, Y. Dai, M. Xie, and J. Hao, Room-temperature ferroelectricity in $MoTe_2$ down to the atomic monolayer limit, Nat. Commun. **10**, 1775 (2019).

[28] F. Liu, L. You, K. L. Seyler, X. Li, P. Yu, J. Lin, X. Wang, J. Zhou, H. Wang, H. He, S. T. Pantelides, W. Zhou, P. Sharma, X. Xu, P. M. Ajayan, J. Wang, and Z. Liu, Room-temperature ferroelectricity in $CuInP_2S_6$ ultrathin flakes, Nat. Commun. **7**, 12357 (2016).

[29] K. Yasuda, X. Wang, K. Watanabe, T. Taniguchi, and P. Jarillo-Herrero, Stacking-engineered ferroelectricity in bilayer boron nitride, Science **372**, 1458 (2021).

[30] M. Vizner Stern, Y. Waschitz, W. Cao, I. Nevo, K. Watanabe, T. Taniguchi, E. Sela, M. Urbakh, O. Hod, and M. Ben Shalom, Interfacial ferroelectricity by van der Waals sliding, Science **372**, 1462 (2021).

[31] X. Wang, K. Yasuda, Y. Zhang, S. Liu, K. Watanabe, T. Taniguchi, J. Hone, L. Fu, and P. Jarillo-Herrero, Interfacial ferroelectricity in rhombohedral-stacked bilayer transition metal dichalcogenides, arXiv:2108.07659.

[32] K. Chang, J. Liu, H. Lin, N. Wang, K. Zhao, A. Zhang, F. Jin, Y. Zhong, X. Hu, W. Duan, Q. Zhang, L. Fu, Q.-K. Xue, X. Chen, and S.-H. Ji, Discovery of robust in-plane ferroelectricity in atomic-thick SnTe, Science **353**, 274 (2016).

[33] C. Zheng, L. Yu, L. Zhu, J. L. Collins, D. Kim, Y. Lou, C. Xu, M. Li, Z. Wei, Y. Zhang, M. T. Edmonds, S. Li, J. Seidel, Y. Zhu, J. Z. Liu, W.-X. Tang, and M. S. Fuhrer, Room temperature in-plane ferroelectricity in van der Waals In_2Se_3, Sci. Adv. **4**, eaar7720 (2018).

[34] K. Chang, F. Küster, B. J. Miller, J.-R. Ji, J.-L. Zhang, P. Sessi, S. Barraza-Lopez, and S. S. P. Parkin, Microscopic manipulation of ferroelectric domains in SnSe monolayers at room temperature, Nano Lett. **20**, 6590 (2020).

[35] N. Higashitarumizu, H. Kawamoto, C.-J. Lee, B.-H. Lin, F.-H. Chu, I. Yonemori, T. Nishimura, K. Wakabayashi, W.-H. Chang, and K. Nagashio, Purely in-plane ferroelectricity in monolayer SnS at room temperature, Nat. Commun. **11**, 2428 (2020).

[36] A. K. Singh and R. G. Hennig, Purely in-plane ferroelectricity in monolayer SnS at room temperature, Appl. Phys. Lett. **105**, 042103 (2014).

[37] R. Fei, W. Li, J. Li, and L. Yang, Giant piezoelectricity of monolayer group IV monochalcogenides: SnSe, SnS, GeSe, and GeS, Appl. Phys. Lett. **107**, 173104 (2015).

[38] R. Fei, W. Kang, and L. Yang, Ferroelectricity and Phase Transitions in Monolayer Group-IV Monochalcogenides, Phys. Rev. Lett. **117**, 097601 (2016).

[39] M. Wu and X. C. Zeng, Intrinsic ferroelasticity and/or multiferroicity in two-dimensional phosphorene and phosphorene analogues, Nano Lett. **16**, 3236 (2016).

[40] H. Wang and X. Qian, Two-dimensional multiferroics in monolayer group IV monochalcogenides, 2D Mater. **4**, 015042 (2017).

[41] T. Rangel, B. M. Fregoso, B. S. Mendoza, T. Morimoto, J. E. Moore, and J. B. Neaton, Large Bulk Photovoltaic Effect and Spontaneous Polarization of Single-Layer Monochalcogenides, Phys. Rev. Lett. **119**, 067402 (2017).

[42] S.-D. Guo and Y.-H. Wang, Thermoelectric properties of orthorhombic group IV–VI monolayers from the first-principles calculations, J. Appl. Phys. **121**, 034302 (2017).

[43] A. I. Lebedev, Ferroelectricity and piezoelectricity in monolayers and nanoplatelets of SnS, J. Appl. Phys. **124**, 164302 (2018).

[44] Y. Bao, P. Song, Y. Liu, Z. Chen, M. Zhu, I. Abdelwahab, J. Su, W. Fu, X. Chi, W. Yu, W. Liu, X. Zhao, Q.-H. Xu, M. Yang, and K. P. Loh, Gate-tunable in-plane ferroelectricity in few-layer SnS, Nano Lett. **19**, 5109 (2019).

[45] S. Barraza-Lopez, B. M. Fregoso, J. W. Villanova, S. S. P. Parkin, and K. Chang, *Colloquium*: Physical properties of group-IV monochalcogenide monolayers, Rev. Mod. Phys. **93**, 011001 (2021).

[46] J. P. Perdew, K. Burke, and M. Ernzerhof, Generalized Gradient Approximation Made Simple, Phys. Rev. Lett. **77**, 3865 (1996).

[47] X. Gonze, J.-M. Beuken, R. Caracas, F. Detraux, M. Fuchs, G.-M. Rignanese, L. Sindic, M. Verstraete, G. Zerah, F. Jollet, M. Torrent, A. Roy, M. Mikami, Ph. Ghosez, J.-Y. Raty, and D. C. Allan, First-principles computation of material properties: the ABINIT software project, Comput. Mater. Sci. **25**, 478 (2002).

[48] D. R. Hamann, Optimized norm-conserving Vanderbilt pseudopotentials, Phys. Rev. B **88**, 085117 (2013).

[49] M. J. van Setten, M. Giantomassi, E. Bousquet, M. J. Verstraete, D. R. Hamann, X. Gonze, and G.-M. Rignanese, The PseudoDojo: Training and grading a 85 element optimized norm-conserving pseudopotential table, Comput. Phys. Commun. **226**, 39 (2018).

[50] R. W. Nunes and X. Gonze, Berry-phase treatment of the homogeneous electric field perturbation in insulators, Phys. Rev. B **63**, 155107 (2001).

[51] I. Souza, J. Íñiguez, and D. Vanderbilt, First-Principles Approach to Insulators in Finite Electric Fields, Phys. Rev. Lett. **89**, 117602 (2002).

[52] J. W. Zwanziger, J. Galbraith, Y. Kipouros, M. Torrent, M. Giantomassi, X. Gonze, Finite homogeneous electric fields in the projector augmented wave formalism: Applications to linear and nonlinear response, Comput. Mater. Sci. **58**, 113 (2012).

[53] Note that we used the relaxed structures from norm-conserving pseudopotentials within PBE but used the local density approximation (LDA) to calculate the EO tensor since such calculation is only implemented within LDA.

[54] M. Abarkan, M. Aillerie, N. Kokanyan, C. Teyssandier, and E. Kokanyan, Electro-optic and dielectric properties of zirconium-doped congruent lithium–niobate crystals, Opt. Mater. Express **4**, 179 (2014).

[55] M. Abarkan, A. Danielyan, N. Kokanyan, M. Aillerie, S. Kostritskii, and E. Kokanyan, The clamped and unclamped effective electro-optic coefficients of zirconium-doped congruent lithium niobate crystals, J. Phys.: Conf. Ser. **879**, 012004 (2017).

[56] P. Günter and M. Zgonik, Clamped–unclamped electro-optic coefficient dilemma in photorefractive phenomena, Opt. Lett. **16**, 1826 (1991).

[57] G. Montemezzani, M. Aillerie, X. Zheng, H. Remmach, and A. A. Grabar, Third column electro-optical coefficients of monoclinic $Sn_2P_2S_6$, Opt. Mater. Express **2**, 920 (2012).

[58] H. Wiedemeier and H. G. V. Schnering, Refinement of the structures of GeS, GeSe, SnS and SnSe, Z. Kristallogr. **148**, 295 (1978).

[59] R. D. King-Smith and D. Vanderbilt, Theory of polarization of crystalline solids, Phys. Rev. B **47**, 1651(R) (1993).

[60] R. Resta, Macroscopic polarization in crystalline dielectrics: the geometric phase approach, Rev. Mod. Phys. **66**, 899 (1994).

[61] J. F. Nye, *Physical Properties of Crystals: Their Representation by Tensors and Matrices* (Oxford University Press, Oxford, 1985).

[62] See Supplemental Material at [URL will be inserted by publisher] for more details about (i) the expression of the dielectric constant in two-dimensional materials; (ii) the derivations of the analytical formula for the EO coefficients in 2D materials; (iii) anticrossings; (iv) electric field applied along the direction that is opposite to the initial spontaneous polarization direction; and (v) electro-optic coefficients in monolayer SnSe.

[63] A. Laturia, M. L. Van de Put, and W. G. Vandenberghe, npj 2D Mater. Appl. **2**, 6 (2018).

[64] H. Y. Zhang, X. H. He, Y. H. Shih, S. H. Tang, A new method for measuring the electro-optic coefficients with higher sensitivity and higher accuracy, Opt. Commun. **86**, 509 (1991).

[65] P. Bernasconi, M. Zgonik, and P. Günter, Temperature dependence and dispersion of electro-optic and elasto-optic effect in perovskite crystals, J. Appl. Phys. **78**, 2651 (1995).

[66] M. J. Gunning, R. E. Raab, and W. Kucharczyk, Magnitude and nature of the quadratic electro-optic effect in potassium dihydrogen phosphate and ammonium dihydrogen phosphate crystals, J. Opt. Soc. Am. B **18**, 1092 (2001).